OASIS-3: IMAGING METHODS AND DATA DICTIONARY

VERSION 1.5 MARCH 2018

CONTENTS

INTRODUCTION & CONTACT INFORMATION

OASIS-3 is the latest release in the *Open Access Series of Imaging Studies (OASIS)* that aimed at making neuroimaging datasets freely available to the scientific community. By compiling and freely distributing this multi-modal dataset, we hope to facilitate future discoveries in basic and clinical neuroscience. Previously released data for OASIS-Cross-sectional (Marcus et al, 2007) and OASIS-Longitudinal (Marcus et al, 2010) have been utilized for hypothesis driven data analyses, development of neuroanatomical atlases, and development of segmentation algorithms. OASIS-3 is a longitudinal neuroimaging, clinical, cognitive, and biomarker dataset for normal aging and Alzheimer's Disease.

The OASIS datasets hosted by central.xnat.org provide the community with open access to a significant database of neuroimaging and processed imaging data across a broad demographic, cognitive, and genetic spectrum an easily accessible platform for use in neuroimaging, clinical, and cognitive research on normal aging and cognitive decline. All data is available via www.oasis-brains.org.

OASIS-3 is a retrospective compilation of data for >1000 participants that were collected across several ongoing projects through the WUSTL Knight ADRC over the course of 30years. Participants include 609 cognitively normal adults and 489 individuals at various stages of cognitive decline ranging in age from 42-95yrs. All participants were assigned a new random identifier and all dates were removed and normalized to reflect days from entry into study. The dataset contains over 2000 MR sessions which include T1w, T2w, FLAIR, ASL, SWI, time of flight, resting-state BOLD, and DTI sequences. Many of the MR sessions are accompanied by volumetric segmentation files produced through Freesurfer processing. PET imaging from 3 different tracers, PIB, AV45, and FDG, totaling over 1500 raw imaging scans and the accompanying post-processed files from the Pet Unified Pipeline (PUP) are also available in OASIS-3.

ACCESS TO OASIS-3

Access to OASIS imaging, clinical, and biomarker data is available for access after completing the Data Use Agreement. Please log all data access requests using the online forms at www.oasis-brains.org.

- Data is available for access at https://central.xnat.org
- Further resources, including updated copies of this Data Dictionary, are available online at www.oasis-brains.org.
- Both OASIS: Cross-Sectional (OASIS-1) and OASIS: Longitudinal (OASIS-2) are available at https://central.xnat.org.
- CONTACT INFORMATION: oasis-brains@nrg.wustl.edu

OASIS PROJECTS

Each OASIS project should be used independently and not combined. Due to anonymization participants may be included in all three datasets under unique IDs.

- OASIS-1: Cross-Sectional T1w MR images across the lifespan (ages 18-96) with dementia status (doi: 10.1162/jocn.2007.19.9.1498)
- OASIS-2: Longitudinal T1w MR images in older adults (ages 60-96) with dementia status (doi: 10.1162/jocn.2009.21407)
- OASIS-3: Longitudinal MR and PET images (ages 42-95) with dementia status

DATA RELEASES

RELEASE 1.0: MARCH 2018

- 1098 Subjects (age 42-95)
- Neuroimaging:
    - 2118 MR Sessions
        - 1912 Freesurfer processed outputs
    - *(TBD)* PET Sessions
        - 1356 PET Unified Pipeline processed outputs
- Clinical and Cognitive Measures:
    - 6217 Longitudinal Clinical follow-up assessments
    - 3342 Neuropsychological Assessments
    - 4089 NACC UDS Assessments

USING CENTRAL.XNAT.ORG

SEARCHING, REPORTING, AND DATA MINING:

- **Standard Search**: https://wiki.xnat.org/documentation/how-to-use-xnat/using-the-standard-search
- **Using the Advanced Search**: https://wiki.xnat.org/documentation/how-to-use-xnat/using-the-standard-search/using-the-advanced-search
- **Saving a Data Table as a Stored Search**: https://wiki.xnat.org/documentation/how-to-use-xnat/using-the-standard-search/saving-a-data-table-as-a-stored-search
- **How to Edit, Filter, and Join Tables**: https://wiki.xnat.org/documentation/how-to-use-xnat/using-the-standard-search/how-to-edit-filter-and-join-data-tables

DOWNLOADING DATA

- **How to Download Files via the XNAT REST API (*recommended*)**: https://wiki.xnat.org/display/XAPI/How+To+Download+Files+via+the+XNAT+REST+API
- **How to Download Images from UI:** https://wiki.xnat.org/documentation/how-to-use-xnat/how-to-download-image-data-from-xnat-projects
- **Troubleshooting XNAT Java Applet Issues**: https://wiki.xnat.org/documentation/how-to-use-xnat/image-session-upload-methods-in-xnat/troubleshooting-xnat-java-applet-issues

DEMOGRAPHICS

TABLE 1. SUBJECT DEMOGRAPHICS

	N	AGE	Right Handed
F	611	67.78 (43.2-95.6)	546
M	487	70.17 (42.5-91.7)	433
Total	1098	68.84 (42.5-95.6)	979

TABLE 2. CLINICAL DEMENTIA RATING (CDR)

	max CDR					
min CDR	**0**	**0.5**	**1**	**2**	**3**	Grand Total
0	609*	192	39	12	2	854
0.5		66	61	45	5	177
>1			31	31	5	67
Grand Total	**609**	**258**	**131**	**88**	**12**	**1098**

Unchanged CDR = 0 represents cognitively healthy population

OASIS FILE DESCRIPTION

BIDS FILE SPECIFICATION

All MR and PET imaging files are converted to nifti format utilizing the BIDS format (Gorgolewski et al., 2016). This allows for standardized naming and file formats. Raw MR files, in DICOM or IMA format were converted to Nifti format using dcm2nii (DICOM=dcm2niix v1.0.20171017 and IMA=dcm2nii mricronlx64-2013.06.12; Li et al., 2016). In addition to nifti files, a supplemental json file is included with additional acquisition header information, such as TR, TE, flip angle, and scanner model, that is absent from nifti headers.

Documentation on BIDS can be found here (http://bids.neuroimaging.io/).

***Nifti conversion was completed after volumetric processing that has two big implications.**

- **First, any new processing of T1w.nii images through Freesurfer will result in different values as documented in FreeSurfer regarding file format changes.**
- **Second, the T1.mgz associated with the OASIS-3 Freesurfer processing is the result of dicom conversion to mgz and can be used in place of the T1w.nii file for comparative FreeSurfer processing.**

MR IMAGES

- anat
  - T1w
  - T2w
  - TSE (acq-TSE_T2w)
  - T2star
  - FLASH
  - Flair
  - Time of Flight (acq-TOF_angio)
- func
  - Task-rest_bold
  - ASL
- fmap
  - Fieldmap
- dwi
  - DWI
  - bvec (vector table)
  - bval (vector of b-values)

- swi
  - Magnitude (part-Mag_GRE)
  - Phase (part-Phase_GRE)
  - Minimum Intensity Projection (minIP)
  - SWI

PET IMAGES

- pet
  - raw data coming soon, see below for processed data

TABLE 3A-C. SCAN TYPE INVENTORY

Scan Type	1.5T MR Sessions	3.0T MR Sessions	Total # of MR Session
T1w	236	1881	2117
T2w	230	1755	1985
FLAIR	0	735	735
Bold – Resting State	2	1689	1691
DTI	0	1205	1205
ASL	0	722	722
SWI	2	1217	1219
TOF	1	507	508
Fieldmap	2	977	979

	HR+	PET/CT	PET/MR	Total
PIB				TBD
AV45				TBD
Total				TBD

	Post-Processed Data
FreeSurfer	
5.0/5.1	211
5.3	1701
PUP	
PIB	939
AV45	419
FDG	TDB
Centiloid (Amyloid)	1358

FIGURE 1. LONGITUDINAL IMAGING

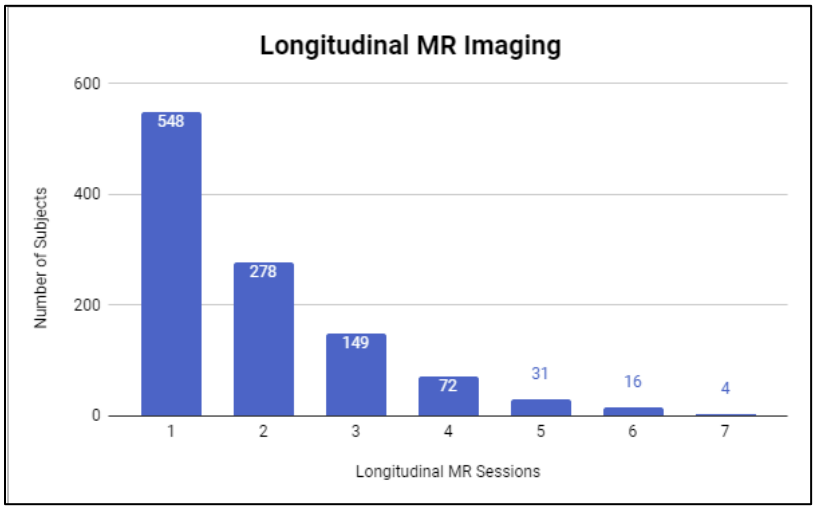

Longitudinal Amyloid PET Imaging

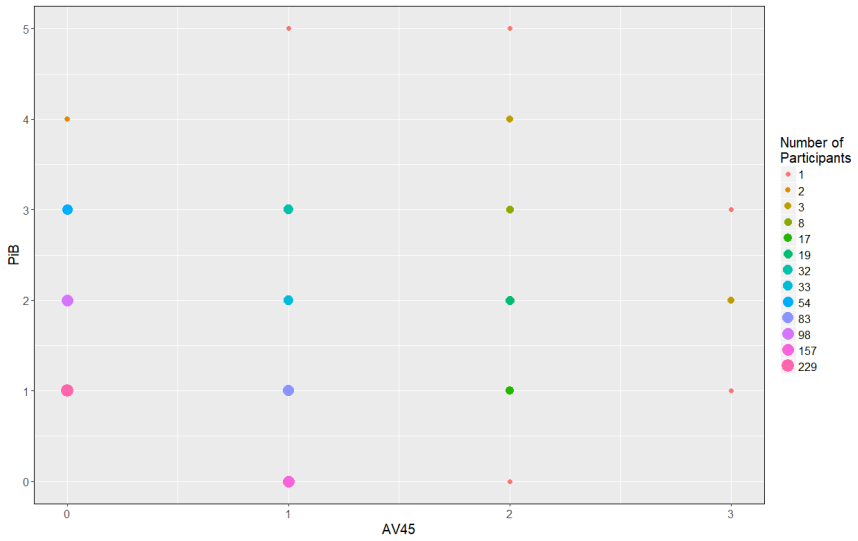

MR IMAGING

MR SCANNERS

Data included in OASIS was collected on the following scanners. Scanner specific information is recorded in dataset_description.json for each MR scan session. *For manuscripts, select only the scanner(s) from which your subset of data were derived.*

- Siemens BioGraph mMR PET-MR 3T scanner
- Siemens TIM Trio 3T MRI scanner (2 scanners)
- Siemens Sonata 1.5T scanner
- Siemens Vision 1.5T scanner

SCANNING METHODS

- Participants were placed in the scanner head to foot while lying in the supine position.
- Head immobilization was done by placing small foam cushions between the head and the head coil.
- In many participants, a Vitamin E capsule was used to mark the left temple.
- For all scans a 16-channel head coil was used.
- Participants receiving simultaneous PET acquisition, on the BioGraph mMR were injected with tracer prior to initiation of MRI scanning
- *Note that not all subjects will have every type of image data.*

DTI IMAGING

The OASIS-3 dataset includes 1205 DTI. All sequences include a *bvec and *bval file that includes information on the vectors and b-values as estimated through the dcm2niix conversion. These files are found in the BIDS folder associated with the DTI nifti. DTI sequences collected on Siemens scanners are known to have a variance of +/- 10%. Below is the standard vector table for Siemens 25-direction DTI.

VECTOR TABLE FOR 25 DIRECTIONS

CoordinateSystem = xyz
Normalisation = none
Vector[0] = (-0.200000, 0.000000, 0.000000)
Vector[1] = (-0.457663, 0.000000, -0.174796)
Vector[2] = (-0.619678, 0.000000, 0.236674)
Vector[3] = (-0.647200, -0.420560, 0.210320)
Vector[4] = (-0.529196, -0.529196, -0.529196)
Vector[5] = (-0.163313, 0.163313, -0.163313)
Vector[6] = (-0.305531, 0.305531, 0.305531)
Vector[7] = (-0.346410, 0.589382, 0.112583)
Vector[8] = (-0.294225, -0.770361, 0.000000)
Vector[9] = (-0.334708,-0.876353, 0.000000)
Vector[10] = (-0.107041, -0.294691, 0.147328)
Vector[11] = (-0.174797, 0.000000, -0.538023)
Vector[12] = (-0.222823, 0.000000, 0.685848)
Vector[13] = (0.000000, -0.446071, 0.721758)
Vector[14] = (0.000000, -0.815963, -0.504234)
Vector[15] = (0.000000, -0.142720, -0.373680)
Vector[16] = (0.000000, 0.214080, -0.560520)
Vector[17] = (0.231234, -0.636606, 0.318265)
Vector[18] = (0.435890, -0.458295, -0.599959)
Vector[19] = (0.489898, 0.515079, 0.674296)
Vector[20] = (0.223607, 0.380445, 0.072672)
Vector[21] = (0.365180, 0.365180, -0..365180)
Vector[22] = (0.626649, -0.407205, 0.203641)
Vector[23] = (0.723592, 0.000000, -0.525744)
Vector[24] = (0.809004, 0.000000, 0.587803)

POST-PROCESSED MRI: VOLUMETRIC SEGMENTATION

Single T1w MRI images were processed through Freesurfer to provide volumetric MRI data and segmentations maps. These maps can be used for a variety of purposes such as determining cortical volumes or regions of interest (ROIs) for PET imaging.

FREESURFER

OASIS-3 is a retrospective project that required anonymization of all files. In order to anonymize FreeSurfer output the following were removed: dates, timestamps, QC staff, raw file paths, original directory paths, ID change, and removal of all logs. OASIS-3 provides volumetric values representing Surface Measures from the aparc.stats Freesurfer output file and Subcortical Segmentation from the aseg.stats Freesurfer output file. These can be downloaded in csv format. All additional files, t1.mgz, brainmasks, segmentations, surface maps, and regional statistics.

> ***Conversion to BIDS format was completed following FreeSurfer processing. Segmantation of nifti files will produce different values than segmentation completed on dicom files and is documented by FreeSurfer. Direct comparison to OASIS-3 FreeSurfer files should be done using the T1.mgz file.***

For a full description of Subcortical Segmentation and Surface Measures statistical variable see list.

PROCESSING BACKGROUND

FreeSurfer (http://surfer.nmr.mgh.harvard.edu/) analyses involved cortical reconstruction and volumetric segmentation of T1 weighted images. The technical details of these procedures are described in prior publications (Dale et al., 1999; Dale and Sereno, 1993; Fischl and Dale, 2000; Fischl et al., 2001; Fischl et al., 2002; Fischl et al., 2004a; Fischl et al., 1999a; Fischl et al., 1999b; Fischl et al., 2004b; Han et al., 2006; Jovicich et al., 2006; Segonne et al., 2004)). The processing pipeline included motion correction and segmentation of the subcortical white matter and deep gray matter volumetric structures on a T1 weighted image (Fischl et al., 2002), intensity normalization, registration to a spherical atlas which utilized individual cortical folding patterns to match cortical geometry across subjects (Fischl et al., 1999b), and parcellation of the cerebral cortex into units based on gyral and sulcal structure (Desikan et al., 2006).

All MRI sessions were processed through the FreeSurfer image analysis suite using Dell PowerEdge 1950 servers with Intel Xeon processors running CentOS 5.5 Linux.

- All 1.5T imaging data was reprocessed using FreeSurfer 5.0 or Freesurfer 5.1.
- All 3.0T MRI imaging data was reprocessed using FreeSurfer 5.3-HCP-patch.
- All data (1.5 and 3.0 T) have been corrected per the 2012 patch released by MGH.

QUALITY CONTROL MEASURES

All individuals were trained in the FreeSurfer quality control measures developed by the WU ADRC Imaging Core prior to interacting with the data. Such measures included processing pipeline workflows, visual inspection of the data for erroneous sessions, and the correct applications of edits to the volumes when errors persist. Additional information surrounding the FreeSurfer quality control process may be found through the FreeSurfer website, http://surfer.nmr.mgh.harvard.edu/fswiki/FsTutorial/TroubleshootingData.

OASIS-3 includes FreeSurfer output for sessions that were of quality “pass” or “pass with edits”.

ANALYSIS CONSIDERATIONS

CORRECTING SUBCORTICAL AND CORTICAL VOLUMES FOR HEAD SIZE

It is suggested that all regions volumes should be corrected for head size (intracranial volume, ICV) in order to have correct comparisons. This does not apply to cortical thickness measures, as cortical thickness does not significantly vary with head size. The normalization process applies to each individual ROI and is sample specific. Please note if participants are removed from the data set the normalizations on the subcortical volumes will need to be re-run.

Note: Volume normalization must be repeated every time a subject is added or removed from the sample.

An analysis of the ICV estimate for each participant was performed on a longitudinal cohort (Figure 2). All participants had MRI scans using a 3T scanner and were processed with FreeSurfer 5.3. Within a participant, ICV can vary from baseline more than 5% with a mean subject standard deviation of 15.75 cm 3.

Relevant publication for the head-size correction:

Randy L. Buckner, Denise Head, Jamie Parker, Anthony F. Fotenos, Daniel Marcus, John C. Morris, and Abraham Z. Snyder A unified approach for morphometric and functional data analysis in young, old, and demented adults using automated atlas-based head size normalization: reliability and validation against manual measurement of total intracranial volume. Neuroimage, 2004.

Figure 2. (A) ICV estimate for each participant in a longitudinal study. Each black circle represents an MR session and the red line represents a longitudinal participant. (B) The relationship between the raw hippocampal volume and the hippocampal volume normalized by ICV.

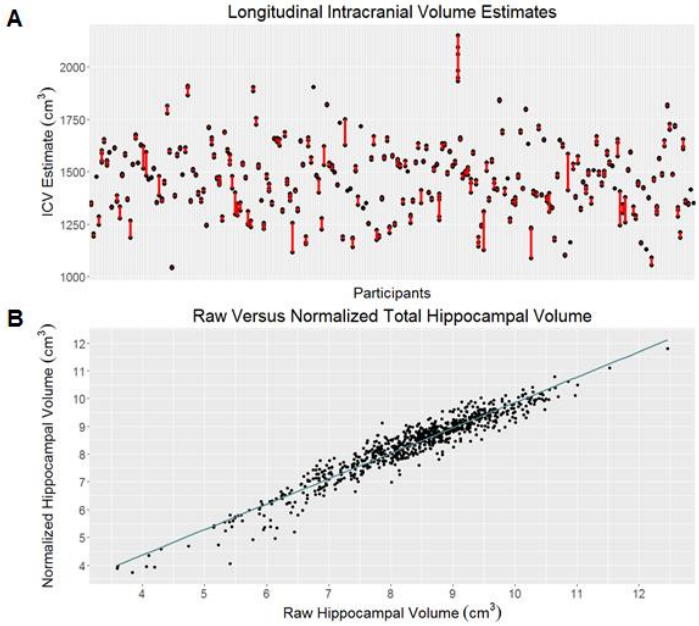

INSTRUCTIONS FOR NORMALIZATION OF MRI FREESURFER-DERIVED CORTICAL VOLUMES

Normalization Calculation:

1. Compute mean ICV for sample
2. Compute regression with ICV as independent variable and ROI as dependent variable to obtain B (NOT Beta) weight
3. Compute: **Normalized = raw volume – (B-weight * (ss ICV – mean ICV))**
   [Note: "ss" = single subject's]
4. This procedure is repeated for each subcortical & cortical ROI volume the investigator is interested in.
   a. These volumes can be found in the "aseg.stats" file.
   b. We do not normalize the cortical thickness measures.

Table 4. below shows a snapshot from the SPSS output for the linear regression. Use the B value highlighted in red for the correction factor. This will be repeated for each given ROI.

Coefficients[a]

Model		Unstandardized Coefficients		Standardized Coefficients	t	Sig.
		B	Std. Error	Beta		
1	(Constant)	2718.207	343.943		7.903	.000
	ICV	-1.513E-5	.000	-.008	-.068	.946

a. Dependent Variable: transtemp

ADDITIONAL REGIONAL CALCULATIONS

Regional FreeSurfer outputs can be combined to generate multiple global brain measures that researchers may find useful (see https://surfer.nmr.mgh.harvard.edu/fswiki/MorphometryStats):

- Whole Brain Volume = Cortex + CorticalWhiteMatter + SubCortGray
- Cortex = lhCortex + rhCortex
- CorticalWhiteMatter = lhCorticalWhiteMatterVol + rhCorticalWhiteMatterVol
- SubCortGray = summation of thalamus, caudate, hippocampus, amygdala, accumbens, ventral DC, substanta nigra (if there). This is a simple voxel count of structures identified as subcortical GM.
- Total Ventricular Volume = left and right lateral inferior lateral ventricles + 3rd + 4th + 5th ventricles)

PET IMAGING

PET SCANNERS

Data included in OASIS was collected on the following scanners. Scanner specific information is recorded in dataset_description.json for each MR scan session. *For manuscripts, select only the scanner(s) from which your subset of data were derived.*

- Siemens Biograph mMR PET-MR 3T scanner (serial#: 51010)
- Siemens Biograph 40 PET/CT scanner (serial#:1003)
- Siemens ECAT HRplus 962 PET scanner

TRACERS

PIB

N-methyl-[^{11}C]2-(4'-methylaminophenyl)-6-hydroxybenzothiazole ([^{11}C]PIB) is a radiolabeled compound that binds *in vivo* to brain amyloid deposits. Developed at the University of Pittsburgh, PIB has very high affinity for amyloid plaques. With administration of 6 - 20 mCi of [^{11}C]PIB, a 60 minute dynamic PET scan in 3D mode (septa retracted) will be initiated (24 x 5 sec frames; 9 x 20 sec frames; 10 x 1 min frames; 9 x 5 min frames).

AV45

Florbetapir binds to β-amyloid (Aβ) plaque utilizing the radioactive isotope 18F for use in PET scanning. Florbetapir F18 is used udner the research number 18F-AV-45 and therefore referred to as AV45. Participants received a single i.v. administration of 370 MBq (10 mCi) of florbetapir F 18 (over 10-60 sec). There are two acceptable procedures for obtaining the florbetapir F 18 PET scans:

1. In the preferred approach, the participant will be positioned in the PET-MR scanner at the time of injection and a 70-minute dynamic scan (with simultaneous PET and full Standard MR acquisition) will be obtained starting at the time of injection. For florbetapir F 18 scans conducted on the PET/MR scanner, a short (approximately 15 minute) CT scan may be conducted on the PET/CT scanner.

2. For those participants who cannot tolerate the full exam, an alternative is to rest quietly in an uptake room for the first 40 minutes after injection. The participant will then be positioned in the PET-MR scanner to undergo a scan lasting 20 minutes, beginning 50 minutes after florbetapir F 18 injection and lasting for 20 minutes, using the Short MR Protocol. For florbetapir F 18 scans conducted on the PET/MR scanner, a short (approximately 15 minute) CT scan may be conducted on the PET/CT scanner.

FDG

Metabolic imaging with [18F]FDG-PET was performed with a 3D dynamic acquisition began 40 minutes after a bolus injection of approximately 5 mCi of FDG and lasted for 20 minutes.

POST-PROCESSED PET: PET UNIFIED PIPELINE (PUP)

PET imaging analyses are performed using the PET unified pipeline (PUP, https://github.com/ysu001/PUP) (Su 2013, Su 2015). PET images are smoothed to achieve a common spatial resolution of 8mm to minimize inter-scanner differences (Joshi et al., 2009). Inter-frame motion correction for the dynamic PET images is performed using standard image registration techniques (Hajnal et al., 1995; Eisenstein et al., 2012). PET-MR registration is performed using a vector-gradient algorithm (VGM; Rowland et al., 2005) in a symmetric fashion (i.e. average transformation for PET->MR and inverse of MR->PET was used as the final transformation matrix). By default, regional PET processing is performed based on FreeSurfer segmentation (using wmparc.mgz as the region definition), and each FreeSurfer region is analyzed. The PET processing pipeline generates both reports of regional measurements as well as an SUVR image in the individual FreeSurfer space.

PUP VARIABLE NOMENCLATURE

Our data naming convention provides a standard for listing the region and the processing method (Table 5a). Left and right brain structures use L and R. When left and right are averaged together the suffix includes the designation TOT. For a full list of variables see PUP Variables. Six prefixes are used:

Table 5a:

Data Type	Definition	Example Name
fBP_	*FreeSurfer calculated Binding Potential*	fBP_TOT_ACCUMBENS
fBP_rsf_	*FreeSurfer calculated, partial volume corrected Binding Potential*	fBP_rsf_TOT_ACCUMBENS
fSUVR_	*FreeSurfer calculated SUVR*	fSUVR_TOT_ACCUMBENS
fSUVR_rsf_	*FreeSurfer calculated, partial volume corrected SUVR,* the gold standard	fSUVR_rsf_TOT_ACCUMBENS

Table 5b:

Tracer	Definition	Example Name
PiB	*[11C]-Pittsburg Compound B*	PiB_fBP_TOT_ACCUMBENS
AV45	*[18F]-Florbetapir*	AV45_fSUVR_TOT_ACCUMBENS

The prefixes (tracer+processed_outcome) are applied to the SAS correlate suffix to create a descriptive SAS compliant name (Table 5b).

- PiB_ fSUVR_rsf_TOT_CTX_PRECUNEUS is the [11C] PiB partial volume corrected SUVR of the gray matter in both the right and left FreeSurfer precuneus.
- PIB_fSUVR_rsf_TOT_WM_PRECUNEUS is the [18F] FDG partial volume corrected SUVR of the white matter calculated using the average activity in both the right and left FreeSurfer precuneus.
- PIB_fBP_TOT_CORTMEAN is the [18F] FDG average BP of the four MCBP cortical structures using FreeSurfer regions (TOTFS_PREFRN, TOTFS_TMP, TOTFS_GYREC, TOT_CTX_PRECUNEUS).

PARTIAL VOLUME CORRECTION

As PET images have low spatial resolution, measured signals are distorted by partial volume effects (PVE). The distortion caused by PVE is a function of the size and shape of the region of interest in addition to spatial resolution of the images. In longitudinal studies, the impact of PVE is further confounded by brain atrophy due to aging and pathological changes. To account for these distortions, correction technique is implemented in our processing pipeline using a regional spread function (RSF; Rousset 1998) based approach (Su 2015). We have demonstrated that the RSF technique was able to improve PET quantification and achieve better sensitivity to longitudinal changes in amyloid burden (Su 2015, 2016). Our standard PET processing includes results both with and without RSF partial volume correction. Also, SUVR images are only available without partial volume correction in current analysis.

AMYLOID PET IMAGING ANALYSIS

Currently, two amyloid imaging tracers are used in our studies, i.e. [11C]-Pittsburgh Compound B (PiB) and [18F]-Florbetapir (AV45). For both tracers, two modeling approaches are implemented: 1) binding potential (BPND) is calculated using Logan graphical analysis (Logan 1996; Mintun 2006; Su 2013, 2015, 2016), when full dynamic PET imaging data are available, i.e. PET acquisition was started in synchronization with tracer administration and PET images were reconstructed into multiple time frames; 2) regional target-to-reference intensity ratio, a.k.a, standard uptake ratio (SUVR), is estimated for all processable PET data. Under standard protocol, quantitative PET analysis (both BPND and SUVR) uses 30 to 60 minutes post-injection as the time window for PiB, and 50 to 70 minutes for AV45; and the cerebellum cortex is used as the default reference region. To assess global amyloid burden based on amyloid PET imaging data, the arithmetic mean of BPND or SUVRs from precuneus (PREC), prefrontal cortex (PREF), gyrus rectus (GR), and lateral temporal (TEMP) regions are defined as the mean cortical binding potential (MCBP) or mean cortical SUVR (MCSUVR). In FreeSurfer based processing, PREC is defined as the combined left and right hemisphere ctx-precuneus, PREF is defined as the left and right combined ctx-superiorfrontal and ctx-rostralmiddlefrontal regions, GR is defined as the left and right combined ctx-lateralorbitofrontal and ctx-medialorbitofrontal regions, and TEMP is defined as the left and right combined ctx-superialtemporal and ctx-middletemporal regions (Fig. 8; Su 2013).

CENTILOID CONVERSION FOR AMYLOID PET

Differences in the amyloid imaging tracer, the PET acquisition, and the analysis protocol across different studies introduce considerable variability within amyloid PET imaging data. This variability leads to difficulties in comparing and interpreting amyloid burden results reported from different groups (Klunk et al, 2015). To achieve comparable results, a standardized scale called Centiloid to convert mean cortical SUVR and BP into a Centiloid measure of *global amyloid disposition*. Regional values are unavailable for this dataset.

The procedure and requirements to define the Centiloid scale is documented in detail in the initial Centiloid paper (Klunk et al 2015). To summarize, the Centiloid scale is defined by two anchor points: the mean amyloid burden measurement of a young control group with no amyloid pathology in their brain, represented as 0 in the Centiloid scale, and the mean amyloid burden of an AD group, represented as 100 in the Centiloid scale (level 1 calibration). Subsequently, a Deming regression and a linear transformation are performed to calibrate the tracer and the local

processing methods to the Centiloid scale (i.e. level 2 calibration). Both PiB and AV45 have been calibrated to the Centiloid scale for both non-partial volume and partial volume correction (rsf) using standard PUP (Su, in prep).

Table 6. Examples of the conversion between non-partial volume corrected SUVR and BP to their respective Centiloid value.

Centiloid Value	PiB 30-60 min BP	PiB 30-60 min SUVR
-10	-0.0442	0.9776
0	0.0347	1.0671
25	0.2320	1.2907
50	0.4294	1.5143
75	0.6267	1.7379
100	0.8240	1.9615
110	0.9029	2.0510

CUTOFF VALUES FOR AMYLOID POSITIVITY

Traditionally, the cutoff for amyloid positivity has been established as MCBP>0.18 based on manually processed PiB data (Mintun 2006). We also established that the same cutoff could be used for FreeSurfer processing generated MCBP based on a study population of 77 participants (Su 2013). Based on this dataset, the cutoff for MCSUVRRSF was determined to be 1.42, the cutoff values for additional versions of global amyloid burden measurements that would generate best matched amyloid positivity classification as using manual MCBP=0.18 are also determined. For AV45, the equivalent cutoff to PiB MCSUVRRSF>1.42 was determined based on a sporadic AD cohort of 103 participants who had AV45-PiB crossover data based on the regression line between AV45 MCSUVRs and PiB MCSUVRRSF (Fig. 3) (Su 2018). The equivalent cutoffs in Centiloid units were also derived by applying the Centiloid conversion equations to the native measurement cutoffs.

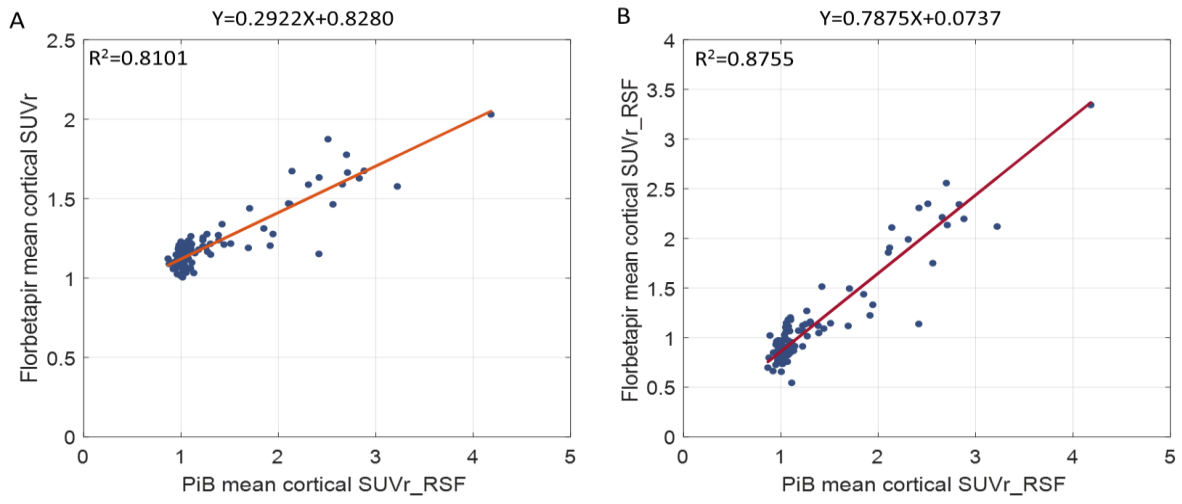

Figure 3. PiB-AV45 crossover dataset illustrating the relationship between AV45 based mean cortical SUVR and PiB based mean cortical SUVRs.

Table 7.

Amyloid Positivity Cutoffs - Cerebellar Cortex Reference Region	
PIB MCBP	0.18
PIB MCBP RSF	0.37
PIB MCSUVR	1.31
PIB MCUSVR RSF	1.42
AV45 MCSUVR	1.24 *
AV45 MCSUVR RSF	1.19 *
Amyloid Positivity Cutoffs – Brainstem Reference Region	
PIB MCSUVR BS	0.79
PIB MCUSVR RSF BS	0.72
Amyloid Positivity Cutoffs - Centiloid	
CL PIB MCBP	18.2
CL PIB MCUSVR RSF	16.4
CL AV45 MCSUVR	21.9
CL AV45 MCSUVR RSF	20.6

* see Su et al 2018.

FREESURFER VARIABLES

Below is a list of the Freesurfer variables as found in OASIS-3 and a suggested list of SAS compatible labels.

MRI Freesurer Default Variable	SAS Compatible Variable Labels
3rd-Ventricle	MR_TOTV_THIRDVENT
4th-Ventricle	MR_TOTV_FOURTHVENT
5th-Ventricle	MR_TOTV_FIFTHVENT
Brain-Stem	MR_TOTV_BRAINSTEM
CC_Anterior	MR_TOTV_CRPCLM_ANT
CC_Central	MR_TOTV_CRPCLM_CNTRL
CC_Mid_Anterior	MR_TOTV_CRPCLM_MID_ANT
CC_Mid_Posterior	MR_TOTV_CRPCLM_MID_POST
CC_Posterior	MR_TOTV_CRPCLM_POST
CortexVol	MR_TOTV_CORTEX
CSF	MR_TOTV_CSF
IntraCranialVol	MR_TOTV_INTRACRANIAL
non-WM-hypointensities	MR_TOTV_NONWMHYPOINTENSITIES
Optic-Chiasm	MR_TOTV_OPTICHIASM
SubCortGrayVol	MR_TOTV_SUBCORTGRAY
TotalGrayVol	MR_TOTV_GRAY
WM-hypointensities	MR_TOTV_WMHYPOINTENSITIES
lh_bankssts_thickness	MR_LT_SSTSBANK
lh_caudalanteriorcingulate_thickness	MR_LT_CAUDANTCNG
lh_caudalmiddlefrontal_thickness	MR_LT_CAUDMIDFRN
lh_cuneus_thickness	MR_LT_CUNEUS
lh_entorhinal_thickness	MR_LT_ENTORHINAL
lh_frontalpole_thickness	MR_LT_FRNPOLE
lh_fusiform_thickness	MR_LT_FUSIFORM
lh_inferiorparietal_thickness	MR_LT_INFRPRTL
lh_inferiortemporal_thickness	MR_LT_INFRTMP
lh_insula_thickness	MR_LT_INSULA
lh_isthmuscingulate_thickness	MR_LT_ISTHMUSCNG
lh_lateraloccipital_thickness	MR_LT_LATOCC
lh_lateralorbitofrontal_thickness	MR_LT_LATORBFRN
lh_lingual_thickness	MR_LT_LINGUAL
lh_medialorbitofrontal_thickness	MR_LT_MEDORBFRN
lh_middletemporal_thickness	MR_LT_MIDTMP
lh_paracentral_thickness	MR_LT_PARACNTRL
lh_parahippocampal_thickness	MR_LT_PARAHPCMPL
lh_parsopercularis_thickness	MR_LT_PARAOPRCLRS
lh_parsorbitalis_thickness	MR_LT_PARSORBLS
lh_parstriangularis_thickness	MR_LT_PARSTRNGLRS
lh_pericalcarine_thickness	MR_LT_PERICLCRN
lh_postcentral_thickness	MR_LT_POSTCNTRL
lh_posteriorcingulate_thickness	MR_LT_POSTCNG
lh_precentral_thickness	MR_LT_PRECNTRL
lh_precuneus_thickness	MR_LT_PRECUNEUS
lh_rostralanteriorcingulate_thickness	MR_LT_ROSANTCNG
lh_rostralmiddlefrontal_thickness	MR_LT_ROSMIDFRN
lh_superiorfrontal_thickness	MR_LT_SUPERFRN
lh_superiorparietal_thickness	MR_LT_SUPERPRTL
lh_superiortemporal_thickness	MR_LT_SUPERTMP
lh_supramarginal_thickness	MR_LT_SUPRAMRGNL
lh_temporalpole_thickness	MR_LT_TMPPOLE
lh_transversetemporal_thickness	MR_LT_TRANSTMP
rh_bankssts_thickness	MR_RT_SSTSBANK
rh_caudalanteriorcingulate_thickness	MR_RT_CAUDANTCNG
rh_caudalmiddlefrontal_thickness	MR_RT_CAUDMIDFRN

rh_cuneus_thickness	MR_RT_CUNEUS
rh_entorhinal_thickness	MR_RT_ENTORHINAL
rh_frontalpole_thickness	MR_RT_FRNPOLE
rh_fusiform_thickness	MR_RT_FUSIFORM
rh_inferiorparietal_thickness	MR_RT_INFRPRTL
rh_inferiortemporal_thickness	MR_RT_INFRTMP
rh_insula_thickness	MR_RT_INSULA
rh_isthmuscingulate_thickness	MR_RT_ISTHMUSCNG
rh_lateraloccipital_thickness	MR_RT_LATOCC
rh_lateralorbitofrontal_thickness	MR_RT_LATORBFRN
rh_lingual_thickness	MR_RT_LINGUAL
rh_medialorbitofrontal_thickness	MR_RT_MEDORBFRN
rh_middletemporal_thickness	MR_RT_MIDTMP
rh_paracentral_thickness	MR_RT_PARACNTRL
rh_parahippocampal_thickness	MR_RT_PARAHPCMPL
rh_parsopercularis_thickness	MR_RT_PARAOPRCLRS
rh_parsorbitalis_thickness	MR_RT_PARSORBLS
rh_parstriangularis_thickness	MR_RT_PARSTRNGLRS
rh_pericalcarine_thickness	MR_RT_PERICLCRN
rh_postcentral_thickness	MR_RT_POSTCNTRL
rh_posteriorcingulate_thickness	MR_RT_POSTCNG
rh_precentral_thickness	MR_RT_PRECNTRL
rh_precuneus_thickness	MR_RT_PRECUNEUS
rh_rostralanteriorcingulate_thickness	MR_RT_ROSANTCNG
rh_rostralmiddlefrontal_thickness	MR_RT_ROSMIDFRN
rh_superiorfrontal_thickness	MR_RT_SUPERFRN
rh_superiorparietal_thickness	MR_RT_SUPERPRTL
rh_superiortemporal_thickness	MR_RT_SUPERTMP
rh_supramarginal_thickness	MR_RT_SUPRAMRGNL
rh_temporalpole_thickness	MR_RT_TMPPOLE
rh_transversetemporal_thickness	MR_RT_TRANSTMP
Left-Accumbens-area	MR_LV_ACCUMBENS
Left-Amygdala	MR_LV_AMYGDALA
Left-Caudate	MR_LV_CAUD
Left-Cerebellum-Cortex	MR_LV_CBLL_CORTEX
Left-Cerebellum-White-Matter	MR_LV_CBLL_WM
Left-choroid-plexus	MR_LV_CHORPLEX
Left-Hippocampus	MR_LV_HIPPOCAMPUS
Left-Inf-Lat-Vent	MR_LV_INFLATVENT
Left-Lateral-Ventricle	MR_LV_LATVENT
Left-non-WM-hypointensities	MR_LV_NONWMHYPOINTENSITIES
Left-Pallidum	MR_LV_PALLIDUM
Left-Putamen	MR_LV_PUTAMEN
Left-Thalamus-Proper	MR_LV_THALAMUS
Left-VentralDC	MR_LV_VENTRALDC
Left-vessel	MR_LV_VESSEL
Left-WM-hypointensities	MR_LV_WMHYPOINTENSITIES
lh_bankssts_volume	MR_LV_SSTSBANK
lh_caudalanteriorcingulate_volume	MR_LV_CAUDANTCNG
lh_caudalmiddlefrontal_volume	MR_LV_CAUDMIDFRN
lh_cuneus_volume	MR_LV_CUNEUS
lh_entorhinal_volume	MR_LV_ENTORHINAL
lh_frontalpole_volume	MR_LV_FRNPOLE
lh_fusiform_volume	MR_LV_FUSIFORM
lh_inferiorparietal_volume	MR_LV_INFRPRTL
lh_inferiortemporal_volume	MR_LV_INFRTMP
lh_insula_volume	MR_LV_INSULA
lh_isthmuscingulate_volume	MR_LV_ISTHMUSCNG
lh_lateraloccipital_volume	MR_LV_LATOCC
lh_lateralorbitofrontal_volume	MR_LV_LATORBFRN
lh_lingual_volume	MR_LV_LINGUAL
lh_medialorbitofrontal_volume	MR_LV_MEDORBFRN
lh_middletemporal_volume	MR_LV_MIDTMP

lh_paracentral_volume	MR_LV_PARACNTRL
lh_parahippocampal_volume	MR_LV_PARAHPCMPL
lh_parsopercularis_volume	MR_LV_PARAOPRCLRS
lh_parsorbitalis_volume	MR_LV_PARSORBLS
lh_parstriangularis_volume	MR_LV_PARSTRNGLRS
lh_pericalcarine_volume	MR_LV_PERICLCRN
lh_postcentral_volume	MR_LV_POSTCNTRL
lh_posteriorcingulate_volume	MR_LV_POSTCNG
lh_precentral_volume	MR_LV_PRECNTRL
lh_precuneus_volume	MR_LV_PRECUNEUS
lh_rostralanteriorcingulate_volume	MR_LV_ROSANTCNG
lh_rostralmiddlefrontal_volume	MR_LV_ROSMIDFRN
lh_superiorfrontal_volume	MR_LV_SUPERFRN
lh_superiorparietal_volume	MR_LV_SUPERPRTL
lh_superiortemporal_volume	MR_LV_SUPERTMP
lh_supramarginal_volume	MR_LV_SUPRAMRGNL
lh_temporalpole_volume	MR_LV_TMPPOLE
lh_transversetemporal_volume	MR_LV_TRANSTMP
lhCortexVol	MR_LV_CORTEX
lhCorticalWhiteMatterVol	MR_LV_CORTICALWM
rh_bankssts_volume	MR_RV_SSTSBANK
rh_caudalanteriorcingulate_volume	MR_RV_CAUDANTCNG
rh_caudalmiddlefrontal_volume	MR_RV_CAUDMIDFRN
rh_cuneus_volume	MR_RV_CUNEUS
rh_entorhinal_volume	MR_RV_ENTORHINAL
rh_frontalpole_volume	MR_RV_FRNPOLE
rh_fusiform_volume	MR_RV_FUSIFORM
rh_inferiorparietal_volume	MR_RV_INFRPRTL
rh_inferiortemporal_volume	MR_RV_INFRTMP
rh_insula_volume	MR_RV_INSULA
rh_isthmuscingulate_volume	MR_RV_ISTHMUSCNG
rh_lateraloccipital_volume	MR_RV_LATOCC
rh_lateralorbitofrontal_volume	MR_RV_LATORBFRN
rh_lingual_volume	MR_RV_LINGUAL
rh_medialorbitofrontal_volume	MR_RV_MEDORBFRN
rh_middletemporal_volume	MR_RV_MIDTMP
rh_paracentral_volume	MR_RV_PARACNTRL
rh_parahippocampal_volume	MR_RV_PARAHPCMPL
rh_parsopercularis_volume	MR_RV_PARAOPRCLRS
rh_parsorbitalis_volume	MR_RV_PARSORBLS
rh_parstriangularis_volume	MR_RV_PARSTRNGLRS
rh_pericalcarine_volume	MR_RV_PERICLCRN
rh_postcentral_volume	MR_RV_POSTCNTRL
rh_posteriorcingulate_volume	MR_RV_POSTCNG
rh_precentral_volume	MR_RV_PRECNTRL
rh_precuneus_volume	MR_RV_PRECUNEUS
rh_rostralanteriorcingulate_volume	MR_RV_ROSANTCNG
rh_rostralmiddlefrontal_volume	MR_RV_ROSMIDFRN
rh_superiorfrontal_volume	MR_RV_SUPERFRN
rh_superiorparietal_volume	MR_RV_SUPERPRTL
rh_superiortemporal_volume	MR_RV_SUPERTMP
rh_supramarginal_volume	MR_RV_SUPRAMRGNL
rh_temporalpole_volume	MR_RV_TMPPOLE
rh_transversetemporal_volume	MR_RV_TRANSTMP
rhCortexVol	MR_RV_CORTEX
rhCorticalWhiteMatterVol	MR_RV_CORTICALWM
Right-Accumbens-area	MR_RV_ACCUMBENS
Right-Amygdala	MR_RV_AMYGDALA
Right-Caudate	MR_RV_CAUD
Right-Cerebellum-Cortex	MR_RV_CBLL_CORTEX
Right-Cerebellum-White-Matter	MR_RV_CBLL_WM
Right-choroid-plexus	MR_RV_CHORPLEX
Right-Hippocampus	MR_RV_HIPPOCAMPUS

Right-Inf-Lat-Vent	MR_RV_INFLATVENT
Right-Lateral-Ventricle	MR_RV_LATVENT
Right-non-WM-hypointensities	MR_RV_NONWMHYPOINTENSITIES
Right-Pallidum	MR_RV_PALLIDUM
Right-Putamen	MR_RV_PUTAMEN
Right-Thalamus-Proper	MR_RV_THALAMUS
Right-VentralDC	MR_RV_VENTRALDC
Right-vessel	MR_RV_VESSEL
Right-WM-hypointensities	MR_RV_WMHYPOINTENSITIES

PUP VARIABLES

Below is a list of the Pet Unified Pipeline (PUP) variables as found in OASIS-3 and a suggested list of SAS compatible labels. The prefixes (tracer+processed_outcome) are applied to the SAS correlate suffix to create a descriptive SAS compliant name (ex: PiB_mSUVR_TOT_ACCUMBENS).

Structure Name	SAS Compatible Variable Labels
Accumbens_area	TOT_ACCUMBENS
Amygdala	TOT_AMYGDALA
Brain_Stem	TOT_BRAINSTEM
Caudate	TOT_CAUD
CC_Anterior	CRPCLM_ANT
CC_Central	CRPCLM_CNTRL
CC_Mid_Anterior	CRPCLM_MID_ANT
CC_Mid_Posterior	CRPCLM_MID_POST
CC_Posterior	CRPCLM_POST
Cerebellum_Cortex	TOT_CBLL_CORTEX
Cerebellum_White_Matter	TOT_CBLL_WM
choroid_plexus	TOT_CHORPLEX
ctx_bankssts	TOT_CTX_SSTSBANK
ctx_caudalanteriorcingulate	TOT_CTX_CAUDANTCNG
ctx_caudalmiddlefrontal	TOT_CTX_CAUDMIDFRN
ctx_corpuscallosum	TOT_CTX_CRPCLM
ctx_cuneus	TOT_CTX_CUNEUS
ctx_entorhinal	TOT_CTX_ENTORHINAL
ctx_frontalpole	TOT_CTX_FRNPOLE
ctx_fusiform	TOT_CTX_FUSIFORM
ctx_inferiorparietal	TOT_CTX_INFERPRTL
ctx_inferiortemporal	TOT_CTX_INFERTMP
ctx_insula	TOT_CTX_INSULA
ctx_isthmuscingulate	TOT_CTX_ISTHMUSCNG
ctx_lateraloccipital	TOT_CTX_LATOCC
ctx_lateralorbitofrontal	TOT_CTX_LATORBFRN
ctx_lh_bankssts	L_CTX_SSTSBANK
ctx_lh_caudalanteriorcingulate	L_CTX_CAUDANTCNG
ctx_lh_caudalmiddlefrontal	L_CTX_CAUDMIDFRN
ctx_lh_corpuscallosum	L_CTX_CRPCLM
ctx_lh_cuneus	L_CTX_CUNEUS
ctx_lh_entorhinal	L_CTX_ENTORHINAL
ctx_lh_frontalpole	L_CTX_FRNPOLE
ctx_lh_fusiform	L_CTX_FUSIFORM
ctx_lh_inferiorparietal	L_CTX_INFRPRTL
ctx_lh_inferiortemporal	L_CTX_INFRTMP
ctx_lh_insula	L_CTX_INSULA
ctx_lh_isthmuscingulate	L_CTX_ISTHMUSCNG
ctx_lh_lateraloccipital	L_CTX_LATOCC
ctx_lh_lateralorbitofrontal	L_CTX_LATORBFRN
ctx_lh_lingual	L_CTX_LINGUAL
ctx_lh_medialorbitofrontal	L_CTX_MEDORBFRN
ctx_lh_middletemporal	L_CTX_MIDTMP
ctx_lh_paracentral	L_CTX_PARACNTRL
ctx_lh_parahippocampal	L_CTX_PARAHPCMPL
ctx_lh_parsopercularis	L_CTX_PARSOPRCLRS
ctx_lh_parsorbitalis	L_CTX_PARSORBLS
ctx_lh_parstriangularis	L_CTX_PARSTRNGLRS
ctx_lh_pericalcarine	L_CTX_PERICLCRN
ctx_lh_postcentral	L_CTX_POSTCNTRL
ctx_lh_posteriorcingulate	L_CTX_POSTCNG
ctx_lh_precentral	L_CTX_PRECNTRL
ctx_lh_precuneus	L_CTX_PRECUNEUS

ctx_lh_rostralanteriorcingulate	L_CTX_ROSANTCNG
ctx_lh_rostralmiddlefrontal	L_CTX_ROSMIDFRN
ctx_lh_superiorfrontal	L_CTX_SUPERFRN
ctx_lh_superiorparietal	L_CTX_SUPERPRTL
ctx_lh_superiortemporal	L_CTX_SUPERTMP
ctx_lh_supramarginal	L_CTX_SUPRAMRGNL
ctx_lh_temporalpole	L_CTX_TMPPOLE
ctx_lh_transversetemporal	L_CTX_TRANSTMP
ctx_lingual	TOT_CTX_LINGUAL
ctx_medialorbitofrontal	TOT_CTX_MEDORBFRN
ctx_middletemporal	TOT_CTX_MIDTMP
ctx_paracentral	TOT_CTX_PARACNTRL
ctx_parahippocampal	TOT_CTX_PARAHPCMPL
ctx_parsopercularis	TOT_CTX_PARSOPCLRS
ctx_parsorbitalis	TOT_CTX_PARSORBLS
ctx_parstriangularis	TOT_CTX_PARSTRNGLS
ctx_pericalcarine	TOT_CTX_PERICLCRN
ctx_postcentral	TOT_CTX_POSTCNTRL
ctx_posteriorcingulate	TOT_CTX_POSTCNG
ctx_precentral	TOT_CTX_PRECNTRL
ctx_precuneus	TOT_CTX_PRECUNEUS
ctx_rh_bankssts	R_CTX_SSTSBANK
ctx_rh_caudalanteriorcingulate	R_CTX_CAUDANTCNG
ctx_rh_caudalmiddlefrontal	R_CTX_CAUDMIDFRN
ctx_rh_corpuscallosum	R_CTX_CRPCLM
ctx_rh_cuneus	R_CTX_CUNEUS
ctx_rh_entorhinal	R_CTX_ENTORHINAL
ctx_rh_frontalpole	R_CTX_FRNPOLE
ctx_rh_fusiform	R_CTX_FUSIFORM
ctx_rh_inferiorparietal	R_CTX_INFPRTL
ctx_rh_inferiortemporal	R_CTX_INFTMP
ctx_rh_insula	R_CTX_INSULA
ctx_rh_isthmuscingulate	R_CTX_ISTHMUSCNG
ctx_rh_lateraloccipital	R_CTX_LATOCC
ctx_rh_lateralorbitofrontal	R_CTX_LATORBFRN
ctx_rh_lingual	R_CTX_LINGUAL
ctx_rh_medialorbitofrontal	R_CTX_MEDORBFRN
ctx_rh_middletemporal	R_CTX_MIDTMP
ctx_rh_paracentral	R_CTX_PARACNTRL
ctx_rh_parahippocampal	R_CTX_PARAHPCMPL
ctx_rh_parsopercularis	R_CTX_PARSOPRCLRS
ctx_rh_parsorbitalis	R_CTX_PARSORBLS
ctx_rh_parstriangularis	R_CTX_PARSTRNGLRS
ctx_rh_pericalcarine	R_CTX_PERICLCRN
ctx_rh_postcentral	R_CTX_POSTCNTRL
ctx_rh_posteriorcingulate	R_CTX_POSTCNG
ctx_rh_precentral	R_CTX_PRECNTRL
ctx_rh_precuneus	R_CTX_PRECUNEUS
ctx_rh_rostralanteriorcingulate	R_CTX_ROSANTCNG
ctx_rh_rostralmiddlefrontal	R_CTX_ROSMIDFRN
ctx_rh_superiorfrontal	R_CTX_SUPERFRN
ctx_rh_superiorparietal	R_CTX_SUPERPRTL
ctx_rh_superiortemporal	R_CTX_SUPERTMP
ctx_rh_supramarginal	R_CTX_SUPRAMRGNL
ctx_rh_temporalpole	R_CTX_TMPPOLE
ctx_rh_transversetemporal	R_CTX_TRANSTMP
ctx_rostralanteriorcingulate	TOT_CTX_ROSANTCNG
ctx_rostralmiddlefrontal	TOT_CTX_ROSMIDFRN
ctx_superiorfrontal	TOT_CTX_SUPERFRN
ctx_superiorparietal	TOT_CTX_SUPERPRTL
ctx_superiortemporal	TOT_CTX_SUPERTMP
ctx_supramarginal	TOT_CTX_SUPRAMRGNL
ctx_temporalpole	TOT_CTX_TMPPOLE

ctx_transversetemporal	TOT_CTX_TRANSTMP
GR_FS	TOTFS_GYREC
Hippocampus	TOT_HIPPOCAMPUS
Left_Accumbens_area	L_ACCUMBENS
Left_Amygdala	L_AMYGDALA
Left_Caudate	L_CAUD
Left_Cerebellum_Cortex	L_CTX_CBLL
Left_Cerebellum_White_Matter	L_WM_CBLL
Left_choroid_plexus	L_CHORPLEX
Left_Hippocampus	L_HIPPOCAMPUS
Left_Pallidum	L_PALLIDUM
Left_Putamen	L_PUTAMEN
Left_Substancia_Nigra	L_SUBSTNCA_NGRA
Left_Thalamus_Proper	L_THALAMUS
Left_UnsegmentedWhiteMatter	L_WM_UNSEGMENTED
Left_VentralDC	L_VENTRALDC
OCC_FS	TOTFS_OCC
Pallidum	TOT_PALLIDUM
PREF_FS	TOTFS_PREFRN
Putamen	TOT_PUTAMEN
Right_Accumbens_area	R_ACCUMBENS
Right_Amygdala	R_AMYGDALA
Right_Caudate	R_CAUD
Right_Cerebellum_Cortex	R_CTX_CBLL
Right_Cerebellum_White_Matter	R_WM_CBLL
Right_choroid_plexus	R_CHORPLEX
Right_Hippocampus	R_HIPPOCAMPUS
Right_Pallidum	R_PALLIDUM
Right_Putamen	R_PUTAMEN
Right_Substancia_Nigra	R_SUBSTNCA_NGRA
Right_Thalamus_Proper	R_THALAMUS
Right_UnsegmentedWhiteMatter	R_WM_UNSEGMENTED
Right_VentralDC	R_VENTRALDC
Substancia_Nigra	TOT_SUBSTNCA_NGRA
TEMP_FS	TOTFS_TMP
Thalamus_Proper	TOT_THALAMUS_PRPR
UnsegmentedWhiteMatter	TOT_WM_UNSEGMENTED
VentralDC	TOT_VENTRALDC
wm_bankssts	TOT_WM_SSTSBNK
wm_caudalanteriorcingulate	TOT_WM_CAUDANTCNG
wm_caudalmiddlefrontal	TOT_WM_CAUDMIDFRN
wm_corpuscallosum	TOT_WM_CRPCLM
wm_cuneus	TOT_WM_CUNEUS
wm_entorhinal	TOT_WM_ENTORHINAL
wm_frontalpole	TOT_WM_FRNPOLE
wm_fusiform	TOT_WM_FUSIFORM
wm_inferiorparietal	TOT_WM_INFERPRTL
wm_inferiortemporal	TOT_WM_INFERTMP
wm_insula	TOT_WM_INSULA
wm_isthmuscingulate	TOT_WM_ISTHMUSCNG
wm_lateraloccipital	TOT_WM_LATOCC
wm_lateralorbitofrontal	TOT_WM_LATORBFRN
wm_lh_bankssts	L_WM_SSTSBANK
wm_lh_caudalanteriorcingulate	L_WM_CAUDANTCNG
wm_lh_caudalmiddlefrontal	L_WM_CAUDMIDFRN
wm_lh_corpuscallosum	L_WM_CRPCLM
wm_lh_cuneus	L_WM_CUNEUS
wm_lh_entorhinal	L_WM_ENTORHINAL
wm_lh_frontalpole	L_WM_FRNPOLE
wm_lh_fusiform	L_WM_FUSIFORM
wm_lh_inferiorparietal	L_WM_INFPRTL
wm_lh_inferiortemporal	L_WM_INFTMP
wm_lh_insula	L_WM_INSULA

wm_lh_isthmuscingulate	L_WM_ISTHMUSCNG
wm_lh_lateraloccipital	L_WM_LATOCC
wm_lh_lateralorbitofrontal	L_WM_LATORBFRN
wm_lh_lingual	L_WM_LINGUAL
wm_lh_medialorbitofrontal	L_WM_MEDORBFRN
wm_lh_middletemporal	L_WM_MIDTMP
wm_lh_paracentral	L_WM_PARACNTRL
wm_lh_parahippocampal	L_WM_PARAHPCMPL
wm_lh_parsopercularis	L_WM_PARSOPRCLRS
wm_lh_parsorbitalis	L_WM_PARSORBLS
wm_lh_parstriangularis	L_WM_PARSTRIANGLRS
wm_lh_pericalcarine	L_WM_PERICLCRN
wm_lh_postcentral	L_WM_POSTCNTRL
wm_lh_posteriorcingulate	L_WM_POSTCNG
wm_lh_precentral	L_WM_PRECNTRL
wm_lh_precuneus	L_WM_PRECUNEUS
wm_lh_rostralanteriorcingulate	L_WM_ROSANTCNG
wm_lh_rostralmiddlefrontal	L_WM_ROSMIDFRN
wm_lh_superiorfrontal	L_WM_SUPERFRN
wm_lh_superiorparietal	L_WM_SUPERPRTL
wm_lh_superiortemporal	L_WM_SUPERTMP
wm_lh_supramarginal	L_WM_SUPRAMRGNL
wm_lh_temporalpole	L_WM_TMPPOLE
wm_lh_transversetemporal	L_WM_TRANSTMP
wm_lingual	TOT_WM_LINGUAL
wm_medialorbitofrontal	TOT_WM_MEDORBFRN
wm_middletemporal	TOT_WM_MIDTMP
wm_paracentral	TOT_WM_PARACNTRL
wm_parahippocampal	TOT_WM_PARAHPCMPL
wm_parsopercularis	TOT_WM_PARSOPRCLRS
wm_parsorbitalis	TOT_WM_PARSORBLS
wm_parstriangularis	TOT_WM_PARSTRNGLRS
wm_pericalcarine	TOT_WM_PERICLCRN
wm_postcentral	TOT_WM_POSTCNTRL
wm_posteriorcingulate	TOT_WM_POSTCNG
wm_precentral	TOT_WM_PRECNTRL
wm_precuneus	TOT_WM_PRECUNEUS
wm_rh_bankssts	R_WM_SSTSBANK
wm_rh_caudalanteriorcingulate	R_WM_CAUDANTCNG
wm_rh_caudalmiddlefrontal	R_WM_CAUDMIDFRN
wm_rh_corpuscallosum	R_WM_CRPCLM
wm_rh_cuneus	R_WM_CUNEUS
wm_rh_entorhinal	R_WM_ENTORHINAL
wm_rh_frontalpole	R_WM_FRNPOLE
wm_rh_fusiform	R_WM_FUSIFORM
wm_rh_inferiorparietal	R_WM_INFERIORPRTL
wm_rh_inferiortemporal	R_WM_INFERIORTMP
wm_rh_insula	R_WM_INSULA
wm_rh_isthmuscingulate	R_WM_ISTHMUSCNG
wm_rh_lateraloccipital	R_WM_LATOCC
wm_rh_lateralorbitofrontal	R_WM_LATORBFRN
wm_rh_lingual	R_WM_LINGUAL
wm_rh_medialorbitofrontal	R_WM_MEDORBFRN
wm_rh_middletemporal	R_WM_MIDTMP
wm_rh_paracentral	R_WM_PARACNTRL
wm_rh_parahippocampal	R_WM_PARAHPCMPL
wm_rh_parsopercularis	R_WM_PARSOPRCLRS
wm_rh_parsorbitalis	R_WM_PARSORBLS
wm_rh_parstriangularis	R_WM_PARSTRNGLRS
wm_rh_pericalcarine	R_WM_PERICLCRN
wm_rh_postcentral	R_WM_POSTCNTRL
wm_rh_posteriorcingulate	R_WM_POSTCNG
wm_rh_precentral	R_WM_PRECNTRL

wm_rh_precuneus	R_WM_PRECUNEUS
wm_rh_rostralanteriorcingulate	R_WM_ROSANTCNG
wm_rh_rostralmiddlefrontal	R_WM_ROSMIDFRN
wm_rh_superiorfrontal	R_WM_SUPERFRN
wm_rh_superiorparietal	R_WM_SUPERPRTL
wm_rh_superiortemporal	R_WM_SUPERTMP
wm_rh_supramarginal	R_WM_SUPRAMRGNL
wm_rh_temporalpole	R_WM_TMPPOLE
wm_rh_transversetemporal	R_WM_TRANSTMP
wm_rostralanteriorcingulate	TOT_WM_ROSANTCNG
wm_rostralmiddlefrontal	TOT_WM_ROSMIDFRN
wm_superiorfrontal	TOT_WM_SUPERFRN
wm_superiorparietal	TOT_WM_SUPERPRTL
wm_superiortemporal	TOT_WM_SUPERTMP
wm_supramarginal	TOT_WM_SUPRAMRGNL
wm_temporalpole	TOT_WM_TMPPOLE
wm_transversetemporal	TOT_WM_TRANSTMP
MCBP	TOT_CORTMEAN

REFERENCES

1. Gorgolewski, K.J., et al. The brain imaging data structure, a format for organizing and describing outputs of neuroimaging experiments. Sci Data 2016; 3:160044. PMID: 27326542 PMCID: PMC4978148 DOI: 10.1038/sdata.2016.44.
2. Li, X, Morgan, P.S., Ashburner, J., Smith, J., Rorden, C. The first step for neuroimaging data analysis: DICOM to NIfTI conversion. J Neurosci Methods 2016; 164:47-56. PMID:26945974 DOI: 10.1016/j.jneumeth.2016.03.001.
3. Chien DT, Bahri S, Szardenings AK, Walsh JC, Mu F, Su M-Y, et al. Early Clinical PET Imaging Results with the Novel PHF-Tau Radioligand [F-18]-T807. J. Alzheimer's Dis. 2013; 34: 457–468.
4. Eisenstein, S.A., Koller, J.M., Piccirillo, M., Kim, A., Antenor-Dorsey, J.A., Videen, T.O., Snyder, A.Z., Karimi, M., Moerlein, S.M., Black, K.J., Perlmutter, J.S., Hershey, T., 2012. Characterization of extrastriatal D2 in vivo specific binding of [(1)(8)F](N-methyl)benperidol using PET. Synapse 66, 770-780.
5. Fischl B. FreeSurfer. *NeuroImage* 2012; 62(2):774-781. PMCID: PMC: 222857
6. Frouin V, Comtat C, Reilhac A, Gre´goire MC. Correction of Partial-Volume Effect for PET Striatal Imaging: Fast Implementation and Study of Robustness. *J Nucl Med* 2002; 43:1715–1726
7. Hajnal, J.V., Saeed, N., Soar, E.J., Oatridge, A., Young, I.R., Bydder, G.M., 1995. A registration and interpolation procedure for subvoxel matching of serially acquired MR images. J Comput Assist Tomogr 19, 289-296.
8. Joshi, A., Koeppe, R.A., Fessler, J.A., 2009. Reducing between scanner differences in multi-center PET studies. Neuroimage 46, 154-159.
9. Klunk WE, Engler H, Nordberg A, Wang,Y, Blomqvist G, Holt DP, Bergstrom M, Savitcheva I, Huang GF, Estrada S, Ausen B, Debnath ML, Barletta J, Price JC, Sandell J, Lopresti BJ, Wall A, Koivisto P, Antoni G, Mathis CA, Langstrom B. Imaging brain amyloid in Alzheimer's disease with Pittsburgh Compound-B. *Ann Neurol* 2004; 55, 306-319.
10. Klunk WE, Koeppe RA, Price JC, Benzinger TL, Devous MD Sr, Jagust WJ, Johnson KA, Mathis CA, Minhas D, Pontecorvo MJ, Rowe CC, Skovronsky DM, Mintun MA. The Centiloid Project: Standardizing quantitative amyloid plaque estimation by PET. *Alzheimer's & Dementia* 2015; 11(1):1-15.e4.
11. Logan J, Fowler AH, Volkow ND. Distribution volume ratios without blood sampling from graphical analysis of PET data. *J Cereb Blood Flow Metab* 1996; 16:834–840.
12. Lopresti BJ, Klunk WE, Mathis CA, Hoge JA, Ziolko SK, Lu X, Meltzer CC, Schimmel K, Tsopelas ND, DeKosky ST, Price JC. Simplified quantification of Pittsburgh Compound B amyloid imaging PET studies: a comparative analysis. *J Nucl Med* 2005; 46:1959-1972.
13. Marcus, DS, Archie, KA, Olsen, T, Ramaratnam, M. The open source neuroimaging research enterprise. *J. Digital Imaging* 2007; 20:130-138.
14. McCormick LM, Ziebell S, Nopoulos P, Cassell M, Andreasen NC, Brumm M. Anterior Cingulate Cortex: An MRI-based parcellation method. *NeuroImage* 2006; 32:1167-1175.
15. Mintun MA, LaRossa GN, Sheline YI, Dence CS, Lee SY, Mach RH, Klunk WE, Mathis CA, DeKosky ST, Morris JC. [11C]PIB in a nondemented population: Potential antecedent marker of Alzheimer disease. *Neurology* 2006; 67;446-452
16. Shruti, M, Gordon BA, Su, Y, Christensen, J, Friedrichsen, K, Jackson K, Hornbeck, R, Balota DM, Cairns, N, Ances, B, Morris, JC. Benzinger TLS. Tau PET imaging in preclinical Alzheimer's Disease: Classifying tau Positivity. *NeuroImage* 2017; 161: 171-178
17. Morris, JC, Roe, CM, Xiong, C, Fagan, AM, Goate, AM, Holtzman, DM, Mintun, MA. APOE predicts amyloid-beta but not tau Alzheimer pathology in cognitively normal aging. *Ann Neurol* 2010; 67:122-131.

18. Ostrowitzki S, Deptula D, Thurfjell L, Barkhof F, Bohrmann B, Brooks DJ, Klunk WE, Ashford E, Yoo K, Xu ZX, Loetscher H, Santarelli L. Mechanism of amyloid removal in patients with Alzheimer disease treated with gantenerumab. *Arch Neurol* 2011; 69:198-207
19. Price TR, Manolio TA, Kronmal RA, Kittner SJ, Yue NC, Robbins J, Anton-Culver H, O'Leary DH. Silent brain infarction on magnetic resonance imaging and neurological abnormalities in community-dwelling older adults. The Cardiovascular Health Study. CHS Collaborative Research Group. *Stroke*. 1997;28(6):1158-64. PMID: 9183343.
20. Robb, R.A., Hanson, D.P., Karwoski, R.A., Larson, A.G., Workman, E.L., Stacy, M.C. Analyze: a comprehensive, operator-interactive software package for multidimensional medical image display and analysis. *Comput Med Imaging Graph* 1989; 13:433-454.
21. Rousset O, Ma Y, Evans A. Correction for partial volume effects in PET: principle and validation. *J Nucl Med* 1998; 39:904–11.
22. Rousset O, Zaidi H. Correction of partial volume effects in emission tomography. In: Zaidi H, ed- itor. Quantitative analysis of nuclear medicine images. New York: Springer; 2006. p. 236–271.
23. Rowland DJ, Garbow JR, Laforest R, Snyder AZ. 2005 Registration of [18F]FDG microPET and small-animal MRI. *Nucl Med Biol* 2005; 32:567-72
24. Sperling RA, Aisen PS, Beckett LA, Bennett DA, Craft S, Fagan AM, Iwatsubo T, Jack CR, Jr., Kaye J, Montine TJ, Park DC, Reiman EM, Rowe CC, Siemers E, Stern Y, Yaffe K, Carrillo MC, Thies B, Morrison-Bogorad M, Wagster MV, Phelps CH. Toward defining the preclinical stages of Alzheimer's disease: recommendations from the National Institute on Aging-Alzheimer's Association workgroups on diagnostic guidelines for Alzheimer's disease. *Alzheimer's & dementia*. 2011;7(3):280-92. PMID: 21514248; PMCID: PMC3220946
25. Su Y, D'Angelo GM, Vlassenko AG, Zhou GF, Snyder AZ, Marcus DS, et al. Quantitative Analysis of PiB-PET with FreeSurfer ROIs. *PLoS One* 2013;8(11):e73377. PMCID: 3819320
26. Su Y, Blazey TM, Snyder AZ, Raichle ME, Marcus DS, Ances BM, Bateman RJ, Cairns NJ, Aldea P, Cash L, Christensen JJ, Friedrichsen K, Hornbeck RC, Farrar AM, Owen CJ, Mayeux R, Brickman AM, Klunk W, Price JC, Thompson PM, Ghetti B, Saykin AJ, Sperling RA, Johnson KA, Schofield PR, Buckles V, Morris JC, Benzinger TL, Network DIA. Partial volume correction in quantitative amyloid imaging. Neuroimage. 2015;107:55-64. PMCID: 4300252.
27. Su Y, Blazey TM, Owen CJ, Christensen JJ, Friedrichsen K, Joseph-Mathurin N, Wang Q, Hornbeck RC, Ances BM, Snyder AZ, Cash LA, Koeppe RA, Klunk WE, Galasko D, Brickman AM, McDade E, Ringman JM, Thompson PM, Saykin AJ, Ghetti B, Sperling RA, Johnson KA, Salloway SP, Schofield PR, Masters CL, Villemagne VL, Fox NC, Forster S, Chen K, Reiman EM, Xiong C, Marcus DS, Weiner MW, Morris JC, Bateman RJ, Benzinger TL, Dominantly Inherited Alzheimer N. Quantitative Amyloid Imaging in Autosomal Dominant Alzheimer's Disease: Results from the DIAN Study Group. PLoS One. 2016;11(3):e0152082. PMCID: PMC4807073.
28. Su Y, Flores S, Wang G, Hornbeck RC, Speidel B, Vlassenko AG, Gordon BA, Mintun MA, Koeppe RA, Klunk WE, McDade E, Xiong C, Morris JC, Bateman R, Benzinger TL. Comparison of Pittsburg Compound B and Florbetapir in Cross-sectional and Longitudinal Studies. 2018. Manuscript in preparation.
29. Talairach J, Tournoux P. Co-planar Stereotaxic Atlas of the Human Brain: 3-D Proportional System: An Approach to Cerebral Imaging. Stuttgart, Germany: Thieme Medical Publishers; 1988.
30. Wahlund LO, Barkhof F, Fazekas F, Bronge L, Augustin M, Sjogren M, Wallin A, Ader H, Leys D, Pantoni L, Pasquier F, Erkinjuntti T, Scheltens P. A new rating scale for age-related white matter changes applicable to MRI and CT. *Stroke*. 2001;32(6):1318-22. PMID: 11387493.